Pergamon

0042-6989(95)00047-X

Vision Res. Vol. 35, No. 21, pp. 3037–3051, 1995

0042-6989/95 $9.50 + 0.00

Testing a Computational Model of Light-adaptation Dynamics

T. E. VON WIEGAND,*† D. C. HOOD,‡ N. GRAHAM‡

Received 16 May 1994; in revised form 2 February 1995

Experiments from the periodic and aperiodic traditions were used to guide the development of a quantitatively valid model of light adaptation dynamics. Temporal contrast sensitivity data were collected over a range of 3 log units of mean luminance for sinusoids of 2 to 50 Hz. Probe thresholds on flashed backgrounds were collected over a range of stimulus-onset asynchronies and background intensities from 0.1 to 1000 td. All experiments were performed foveally in the photopic range and used a consistent stimulus paradigm and psychophysical method. The resulting model represents a merging of elements from both traditions, and consists of a frequency-dependent front-end followed by a subtractive process and static nonlinearity.

Computational model Light adaptation Flicker threshold Probe-flash Stimulus-onset asynchrony

INTRODUCTION

Studies of the dynamics of light adaptation have generally used one of two approaches: periodic (flicker) experiments (de Lange, 1958; Kelly, 1969; Roufs, 1972a,b; and others), or aperiodic experiments using rectangular flashes with superimposed rectangular probes in various timing relationships to the flash (Geisler, 1978; Hood, Ilves, Wandell & Buckingham, 1978; and others). In this paper we use both experimental approaches and develop a model that integrates the results from them.

Some existing models

Periodic models. De Lange's (1952, 1958) application of the theory of linear systems to characterize the human fovea is one of the earliest examples of a periodic model. This approach consolidated much of the flicker psychophysical results that were previously only "taxonomically" addressed (Landis, 1953). It has provided the means by which the essential non-linear aspects of light adaptation could be separated from the linear (filter) aspects.

Models incorporating filter elements based in the periodic tradition are particularly good at capturing the flicker psychophysical data. They are generally constructed along the lines of the model described by Watson (1986). This model of temporal sensitivity contains three stages: a linear filter, asymmetric thresholds for increments and decrements implemented through differential weighting of the increment and decrement signals, and probability summation over time. Another important example of the periodic approach appears in Sperling and Sondhi's (1968) model of luminance discrimination and flicker detection.

Aperiodic models. Weber's law states that the detectable change in light level is approximately proportional to the ambient light level to which the subject has adapted. This law holds for ambient levels from moderate to high intensity, but many conditions in which Weber's law fails are also observable. One such failure involves the change in detection thresholds immediately after a shift in the ambient light level. In one of the earliest demonstrations of this effect, Craik (1938) used stimuli that were presented on momentary steps above or below the adaptation level. Craik's results showed that detection thresholds were higher for momentary steps than for steps that did not return to the pre-stimulus adaptation level.

The probe-flash paradigm was developed to study the non-linearities involved in going from one light level to another (e.g. Geisler, 1978; Hood, 1978; Hood, Finkelstein & Buckingham, 1979; Finkelstein & Hood, 1981; Adelson, 1982; Hood & Finkelstein, 1986; Hayhoe, Benimoff & Hood, 1987; Finkelstein, Harrison & Hood, 1990). Different delays between the onset of a flash background and a test probe were explored to reveal the physiological response saturation (which underlies threshold elevation) and to develop models of how the visual system recovers its sensitivity. These models generally consist of both a multiplicative process

*Research Laboratory of Electronics, Room 36-755, Massachusetts Institute of Technology, 77 Massachusetts Avenue, Cambridge, MA 02139, U.S.A.

†To whom all correspondence should be addressed [*Email* tew@cbgrle.mit.edu].

‡Department of Psychology, Columbia University, New York, NY 10027, U.S.A.

and a subtractive process that develop over time (as the system adapts) followed by a static non-linear function that is related to the physiological response saturation.

Merged models. Each of the above classes of model successfully addresses the empirical data upon which it was based. Generally speaking, periodic models are adept at characterizing small-signal linear phenomenon, while aperiodic models excel in capturing the intrinsic non-linearities involved in shifting from one light level to another.

Graham and Hood (1992b) considered two phenomena, one based in each tradition, that would reveal the strengths and weaknesses of proposed models. The first of these, the background-onset effect, refers to the aperiodic phenomenon in which detection thresholds are elevated when a probe occurs temporally proximal to the onset of a flash and then decrease as the probe is delayed (up to about 200 msec) with respect to the flash onset. The second proposed effect is high temporal frequency linearity, which refers to a phenomenon observable in flicker threshold experiments. At high frequencies, amplitude threshold is relatively unaffected by changes in mean background level. Models from one tradition generally do not pass the test based in the alternate tradition. However, a merged model composed of elements from both traditions can predict both the background-onset effect and high-frequency linearity. Graham and Hood (1992b) did not attempt to produce a quantitative fit to existing data because the experimental conditions differed substantially for data from each tradition. It is known that variations in experimental conditions affect the shapes of these psychophysical curves (see Shapley & Enroth-Cugell, 1984; Hood & Finkelstein, 1986; Watson, 1986; Graham, 1989 for reviews). Here we use a single set of stimulus conditions and test the same subjects to compare directly the results from both approaches. This consistency allows the development of a computational model that combines periodic and aperiodic elements based on these data.

GENERAL METHOD

Subjects

Two observers, 22 and 31 yr of age, were used throughout the three experiments. Neither subject had known color vision defects and their Snellen acuities were 20/20. Subjects were trained in the psychophysical procedure in a series of trial runs of the experiment.

Optical system

The Maxwellian view optical system (Westheimer, 1966) utilized high-output light-emitting diode (LED) light sources. The light source images were constrained to fall within a 1.5 mm dia circle to eliminate occlusion by the iris within the normal range of pupil diameters. The observer's head was immobilized using a dental wax bite bar. This restraint, and the fixation mark described below, allowed consistent orientation of the eye.

Control over the spatial characteristics in each channel was achieved using film images placed one focal length in front of the final lens. The image produced thereby could be viewed by the subject without accommodation [Fig. 1(A) shows the image's appearance].

The radiance of the LEDs was dynamically controllable by computer over approx. 3 log units using a pulse density modulation (PDM) technique (Swanson, Ueno, Smith & Pokorny, 1987). Control signals to each PDM device were derived from the algebraically combined output of three 12-bit digital-to-analog converters (DACs) running at a sample rate of 1000 Hz. Large static shifts beyond the 3 log unit radiance range were produced using neutral density filters. Care was taken to ensure that the pulse density produced by the PDM and the DAC sample rate were always high enough to properly render the stimulus waveforms. Thus, in Expt 1 the number of points per cycle from the DAC varied from a worst case of 20 points at 50 Hz to a nominal 100 points at 10 Hz. In Expts 2 and 3, neutral density filters were used to keep the probe threshold in the range of about 100–5000 pulses per 10 msec probe.

Stimuli

The LED sources were calibrated using a Spectra photometer incorporating a CIE standard photometric filter. Absolute levels were matched between channels, and the linearity of the PDM control input to light output was found to be perfect within measurement error ($r^2 = 0.9965$). Retinal illuminance was estimated using Westheimer's (1966) method.

The dominant wavelengths of the nominally red and green LEDs were calculated from the spectra of the LEDs as measured at the observer's eye position with the film targets in place. The dominant wavelengths were 627 nm (red) and 565 nm (yellow-green) and were essentially on the spectrum locus. The CIE chromaticity coordinates were $x = 0.702$, $y = 0.297$ (red) and $x = 0.412$, $y = 0.585$ (yellow-green). These values are in general agreement with measured values for LEDs in the literature (Watanabe, Mori & Nakamura, 1992; Swanson *et al.*, 1987).

We used a 1 deg (visual angle) test target that had a cosine-amplitude-profile "edge" extending to 2 deg diameter. This target was produced by stops placed in the test and surround channels of the optical system. The slides were photographs of printed random-dot patterns with the appropriate density functions.

Spatial and temporal paradigm. To provide a unified base of data upon which to build a model of light adaptation, stimulus consistency was maintained through the use of a single spatial paradigm in all the experiments. Figures 1(A,B) depict the spatial aspects of the stimulus as they appeared to the observer. The 1 deg diameter circular target was centered in a circular surround field subtending approx. 18 deg visual angle. A central fixation hair-line (not shown in the figure) extended vertically from the top of the field to the center of the target. Figure 1(B) also indicates the temporal relationship between these fields for the three experiments. Further details of the temporal paradigm are described under each experiment's section.

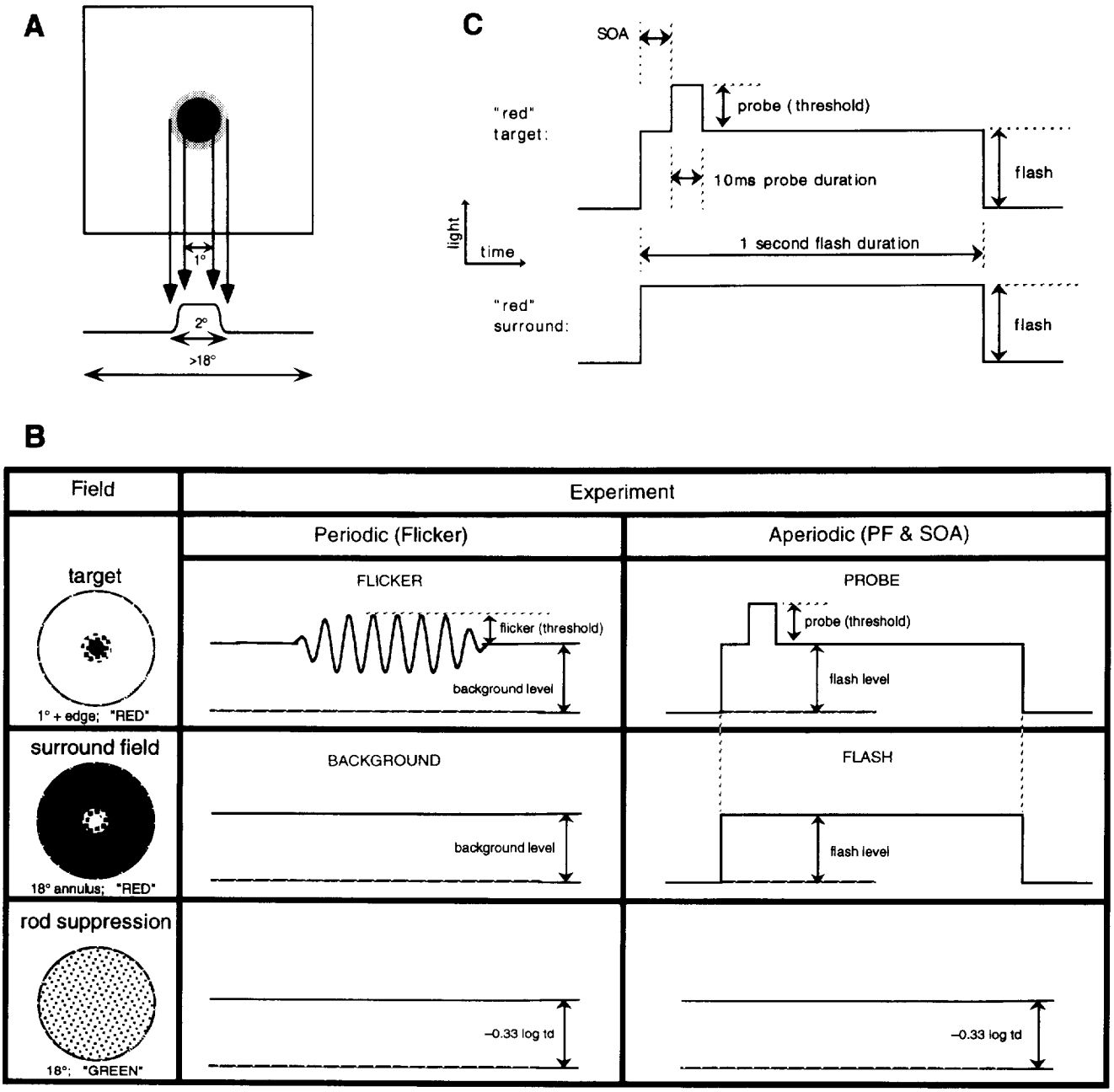

FIGURE 1. Spatial and temporal paradigm for the three experiments. (A) Transmission profile and target in schematic form. (B) Relation between the three superimposed fields for the two types of experiment. (C) Temporal paradigm for the aperiodic experiments in more detail.

Cone isolation. Red LEDs were used as light sources for all stimuli in the experiments in order to minimize the rod contribution. This choice, combined with the foveal location of the stimulation and the mean adapting levels used, ensured minimal rod intrusion. As a further assurance against rod intrusion, the stimuli were presented on a −0.33 log td green LED rod suppression field.

Procedure

The general psychophysical procedure was the same for all experiments. The trials were run using an adaptive psychometric procedure called QUEST (Watson & Pelli, 1983). Responses were collected using a yes/no paradigm. Before each QUEST began, an initial estimate of the detection threshold was provided to the algorithm using the method of adjustment. The QUEST procedure was set up to terminate when the 97.5% confidence level had shrunk to either 0.15 log unit (Expt 1) or 0.3 log unit (Expts 2 and 3). This level was usually reached after the subject completed 12–15 trials for the periodic stimuli of Expt 1, or roughly twice that for the aperiodic stimuli of Expts 2 and 3 (because of the greater variability in response in the aperiodic condition).

A yes/no paradigm was selected over the generally superior forced-choice methodology for two reasons. First, the spatial configuration was not easily adapted to two spatial alternatives and second, the variable (and sometimes lengthy) recovery times in the aperiodic

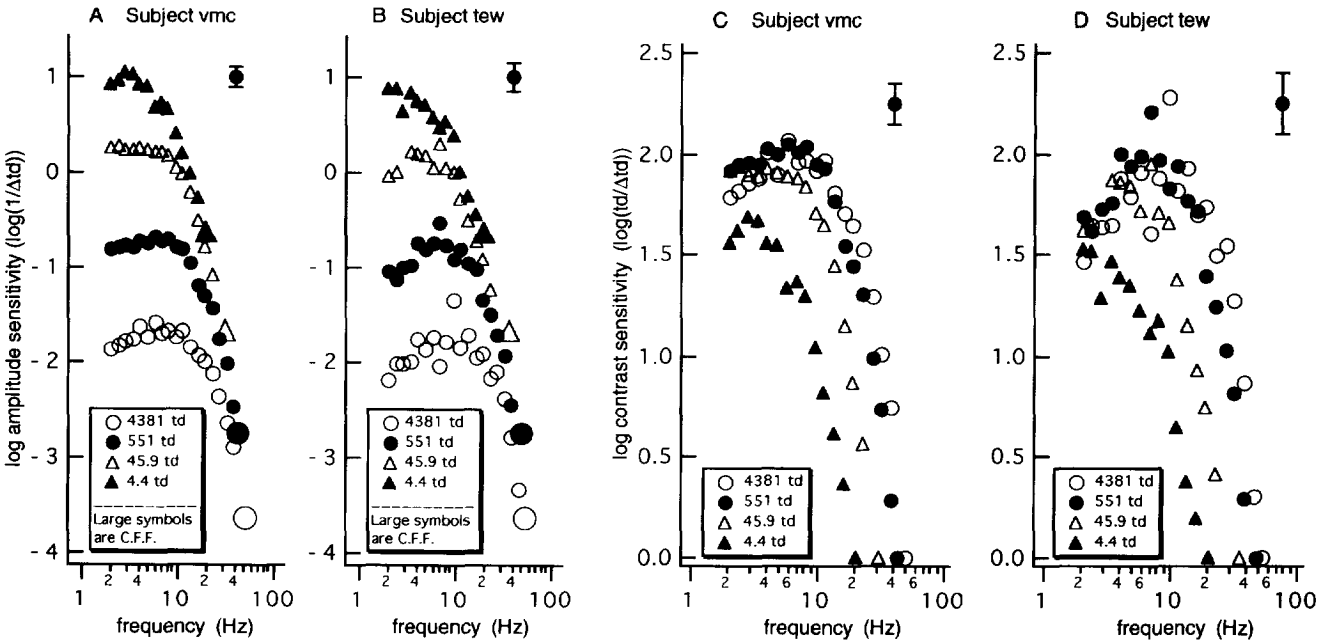

FIGURE 2. Experiment 1 results. (A, B) Amplitude sensitivity vs frequency, parametric in background level for both subjects. Each point is the average of five QUEST determinations of threshold. (C, D) This same data as contrast sensitivity vs frequency, parametric in background level for both subjects. Typical confidence intervals (mean ± 1SE) are shown by the symbols with error bars in the upper-right-hand corner of each panel.

experiments precluded the use of two temporal alternatives.

EXPERIMENT 1

The periodic, or flicker experiment was designed to measure the threshold vs temporal frequency characteristics of the visual system, parametric in mean background level. The current experiment, like de Lange's (1958), involved setting a central target and its surround to some fixed background level to which the subject adapts. The radiance of the target channel was then sinusoidally modulated: the depth of modulation was controlled according to the psychometric algorithm. In Expt 1 the threshold modulation was determined for a number of temporal frequencies. The sequence was repeated at four different background levels.

Method

Stimuli. The spatial and temporal paradigms for this experiment are shown in Fig. 1(B) (periodic). During a trial the central target area was sinusoidally modulated above and below the mean value. The duration of this modulation was either 1 sec for frequencies higher than 4 Hz, or 2 sec for the lower frequencies. In order to minimize the on and off transients, the initial 10% and final 10% of the temporal waveform of the stimulus were shaped by a cosine curve while the middle 80% was steady.

Complete curves were collected at four adapting backgrounds: 4.38, 45.87, 551.5, and 4381 td (0.64, 1.66, 2.74, and 3.64 log td). The independent variable, temporal frequency, was evenly spaced on a logarithmic scale, four points per octave, for five octaves beginning at 2 Hz. The maximum frequency at which 100% modulation could be detected (critical flicker frequency) was determined by presenting a series of high-frequency 100% modulated trials to which the subject responded yes or no.

Procedure. An adaptive QUEST procedure was used as described in the general methods section. For each mean background level, the subject first dark-adapted for 30 min or more, started execution of the control program by pressing a button, then adapted to the background for 10 min. At each background level the temporal frequencies were randomized. An enforced minimum delay of 1 sec between presentations was imposed to control the maximum pace. A reject button was also provided so that the subject could reject a trial in which attention flagged or fixation was lost. This button was used on average about once every 40 presentations.

Results and discussion

Figure 2 shows the results for the two subjects presented both as amplitude sensitivity (A,B) and contrast sensitivity (C,D). Amplitude sensitivity is defined as the reciprocal of the amplitude threshold in trolands, where amplitude is the difference between the peak and mean amplitudes. Contrast sensitivity is the reciprocal of the contrast threshold. Typical confidence intervals (mean ± SE) are shown by the symbols with error bars in the upper-right-hand corner of each panel. These were calculated by pooling the QUEST runs based on a calculation of the SE for the chosen stopping criterion (Appendix in Wiegand, 1993). Notice that subject TEW has a greater variability than the other observer. Presumably the jags in his data just reflect this variability.

The general shape of the curves for both subjects is as expected from previous work. There is a low-pass characteristic with its corner frequency (f_c) moving from about 7 to 12 Hz as the mean background was changed from 4.4 to 4381 td. Also, at the higher backgrounds a peak near f_c becomes prominent.

Two features of the data in Fig. 2 are worth discussing in the context of our efforts to model light adaptation. First, the curves of amplitude sensitivity tend to approach each other at the high-frequency end but they do not actually superimpose. (Actual superimposition would occur if the system were perfectly linear so that the response to flicker of a given amplitude was independent of the background level.) A tendency toward superimposition has been noted before. Indeed, de Lange's (1958) and Kelly's (1972) curves show a similar departure from this perfect linearity though Kelly's data do appear to be more linear. This issue is somewhat clouded by the fact that the experimental curves can only be determined for modulations up to 100%. The determination of high-frequency linearity involves finding a curve that defines a high-frequency linearity envelope through curves that stop at 100% modulation. Inspection of our data can be said to approximate high-frequency linearity.

The second observation is that although the resonant peak exhibited in our data (at around 8-10 Hz) for the highest adapting backgrounds is not as extreme as in de Lange's data, it is in accord with Kelly's data for spatial frequency gratings in the range of 0.5–2.0 c/deg (Kelly, 1972). We make this comparison by assuming our stimulus condition to be roughly comparable to Kelly's 0.5 c/deg grating condition or higher [1 cycle/(1 deg + 1 deg cos edge) ≈ 0.5 c/deg]. Kelly (1959) observed that increasing the target size or removing the background tends to decrease low temporal frequency sensitivity and therefore enhances the observed peak. In general the literature is consistent with this observation (de Lange, 1958; Kelly, 1959; Robson, 1966; van Nes, Koenderink, Nas & Bouman, 1967; Kelly, 1972; Roufs, 1972a, b).

Large sensitivity drops at low temporal frequencies (especially those seen for backgrounds in the 1000–10,000 td range) might suggest a band-pass filter response to some. For example, Watson's (1986) model captures this low temporal frequency fall-off using filters which yield a band-pass response. However, incorporating a low-frequency fall-off characteristic in a model can degrade the Weber's law behavior in the steady state. A more plausible explanation of the peak observed in the data is that it is related to some resonance effect (as in the quadratic filters described below).

EXPERIMENT 2

This experiment in the aperiodic tradition was an exploration of the detection threshold for 10 msec probes superimposed on flashed backgrounds of different levels. Consistent with previous terminology (Hood *et al.*, 1978) this experiment is referred to here as the probe-flash (PF) experiment. The probe was presented at various times following the onset of the flashed background.

Method

Stimuli. The spatial and temporal paradigms for this experiment are shown in Fig. 1(B) (aperiodic). A uniform 18 deg field flashed on for 1 sec. At some time during the flash, a 10 msec probe light appeared superimposed in the central 1 deg (+cosine edge) target area. This probe was triggered after a predetermined delay [the stimulus-onset asynchrony (SOA)].

Complete threshold vs illuminance (TVI) curves were collected at three SOAs. These were 0 and 50 msec and infinity. For each curve, the probe thresholds at 10 flash values were determined. These values were: −1.07, −0.11, 0.54, 1.07, 1.47, 1.71, 2.15, 2.49, 2.79, and 3.05 log td. In the case of the SOA = ∞ condition, the "flashed" background was left on continuously and the subject adapted to each new background for 10 min before the probes were presented. In the case of the SOA < ∞ trials the observer's field contained only the −0.33 log td rod-suppression background, present in all three experiments.

Procedure. An adaptive QUEST procedure was used as described in the General Methods section. For each SOA, the subject first dark-adapted for 30 min or more, started execution of the control program by pressing a button, then adapted to the inter-flash background for 10 min. Within each SOA the flash presentations increased from minimum to maximum in order to preserve light adaptation. The amplitude of the probe was under the control of the QUEST algorithm for determination of the probe threshold. An enforced minimum delay of 8 sec between stimulus presentations was imposed to control the maximum pace of the run. The subject was instructed to wait longer than the 8 sec as needed, to allow afterimages from the probe and flash to fade before beginning the next presentation. For the higher flash levels the time between presentations exceeded 30 sec. The reject button was used somewhat more frequently during this experiment, averaging about once every 20 presentations compared to once in 40 in the flicker experiment.

Results and discussion

Figure 3 shows the results for the two subjects. The data for SOA = ∞ show the transition from a slope of 0.0 at low flash intensities (background has no effect on threshold) to slope 1.0 (Weber's law behavior) at high flash intensities. The transition at just under 1 log td is consistent with the literature (Hood & Finkelstein, 1986). For lower SOAs the slope at high flash intensities is steeper.

While the results for the fully dark-adapted state (SOA = ∞) are fairly typical, there are three aspects of the curves for the non-infinity conditions that deserve further consideration. First, though our thresholds are higher for SOA < ∞ curves than for SOA = ∞ curves, the slopes do not differ appreciably from a slope of 1.0

(Weber's law behavior). Although in previous studies slopes of 1.0 are common for SOA > 0 (e.g. Shevell, 1977; Hood *et al.*, 1978), curves for SOA = 0 are generally reported to be steeper (e.g. Geisler, 1978; Finkelstein *et al.*, 1990; Hayhoe, 1990). This discrepancy can probably be attributed to the numerous differences between the spatial, temporal and chromatic conditions. There are sufficient differences among these studies so that it is not possible to say which is most critical, but one possibility is that the spectral composition is important; previous studies tended to use broadband spectral lights as opposed to pure red LED stimulation. Another possibility (as seen, e.g. in a comparison of Figs 2 and 8 of Hayhoe, Levin & Koshel, 1992) is that the reported slopes are usually fitted to the first 2 log units of data, where they are steeper, and that higher threshold data tend back toward a slope of 1.

Secondly, for SOAs of 0 and 50 msec (as used here), previous studies have shown regions of very high slope when sufficiently intense flashes are used. The flash intensities here were constrained by the use of LEDs. Although over 3 log units above threshold, our flash intensities were still below those used in some previous studies. If we had been able to use higher intensities, we would presumably have found saturation.

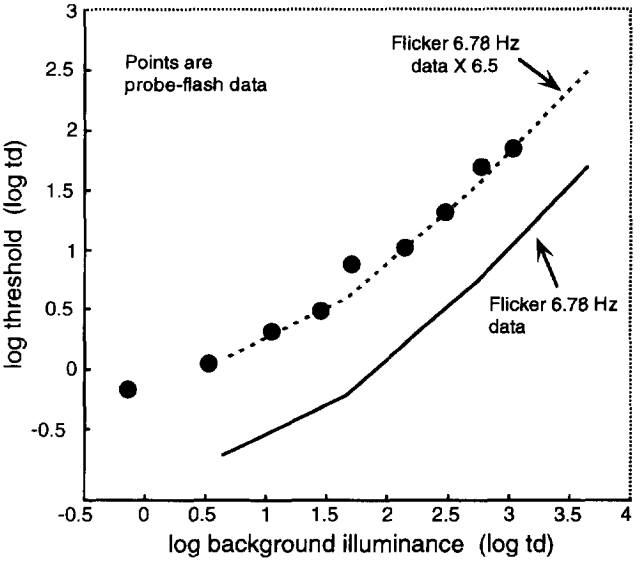

FIGURE 4. Flicker and PF = ∞ data for subject VMC, plotted as TVI, showing the correspondence between periodic and aperiodic data. Points indicate the PF = ∞ thresholds. Solid line indicates the flicker thresholds for a frequency of 6.78 Hz. Dotted line is this same flicker curve multiplied by 6.5 (see text for discussion).

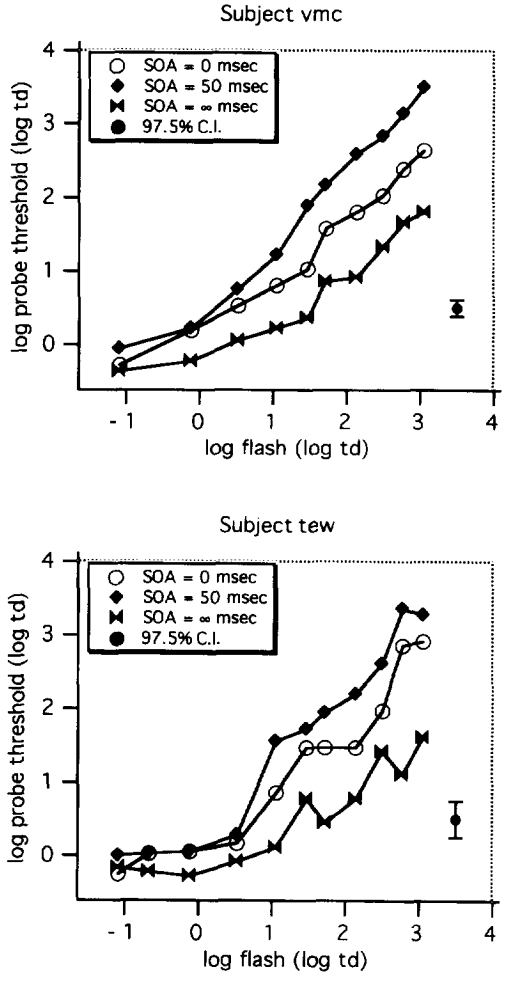

FIGURE 3. Experiment 2 results. Threshold vs illuminance, parametric in SOA. Each point is the average of five QUEST determinations of thresholds for observer VMC and three for observer TEW.

The third notable feature is that the maximal threshold elevation occurs at 50 msec. We decided to explore more thoroughly probe threshold as a function of SOA in a third experiment.

Probe-flash/flicker comparison. An important correspondence between the flicker data of Expt 1 and the probe-flash data of Expt 2 is shown in Fig. 4. The graph shows data for a fully adapted subject (the SOA = ∞ condition) presented as log threshold vs log illuminance. The points indicate the probe-flash thresholds from Expt 2. The solid line indicates the flicker thresholds from Expt 1 for a frequency of 6.78 Hz. The dotted line is this same flicker curve multiplied by 6.5; it matches the probe-flash threshold data well. (The shape of the 6.78 Hz curve gave the best match of the frequencies tested in Expt 1.) There are two processes that may contribute to this factor of 6.5 between the periodic and aperiodic thresholds. First, the "broad-band" 10 msec probe in the probe-flash experiment loses more of its energy through the low-pass action of the visual system than does the sinusoidal 6.78 Hz flicker stimulus. Second, the 1 sec duration flicker may be more detectable because its duration is longer than the 10 msec probe.

This comparison illustrates how our "consistent paradigm" approach can lead to additional insight regarding the extent to which the visual system can be described as a linear system, even before fitting a model. The finding supports the early promise of the linear systems approach (de Lange, 1952). Roufs' (1972a, b) attempt to calculate the exact relation between periodic and aperiodic threshold data resulted only in a qualitative prediction which did not match his empirical measurement.

This was to be expected because he did not take into account (or could not, using only linear filters) the change in detectability of stimuli of different durations. Our data show that the aperiodic thresholds are 6.5 times the periodic, and that the direction of the relation is what would be predicted by Roufs, but without invoking some mechanism to account for the stimulus durations we cannot make quantitative predictions either.

EXPERIMENT 3

In the second aperiodic experiment, referred to simply as the SOA experiment, a finer range of SOAs were tested parametric in flash level. In this form, the experiment most clearly yields information concerning the time course of light adaptation.

Method

This experiment differs from Expt 2 in the order in which the independent variables were varied. A larger number of SOAs at two flash intensities allowed us to focus on the time–course of light adaptation during the first second after a shift in background level. An adaptive QUEST procedure was used as described in the General Methods section. The adaptation timing and inter-trial imposed minimum period were as described for Expt 2.

Stimuli. Complete SOA curves were collected at two flash levels: 1.5 and 2.5 log td. For each level, the probe thresholds at 10 SOA values were determined. These values (in msec) were: 0, 10, 25, 50, 60, 100, 250, 500, 750, and infinity. The SOA was randomized within a run for the non-infinity values.

Results and discussion

Figure 5 shows the data for the two subjects. The general shape of the curves is the same for both. Threshold reaches a maximum at 50 msec and then declines with further increases in SOA. Consistent with Expt 2, there is a maximum at 50 msec. The paradigm here is similar to the classic study of Crawford (1947), but Crawford found that threshold elevation is maximal at 0 msec SOA. Others have reported peak threshold elevations at SOAs both of 0 msec (Boynton & Kandel, 1957; Battersby & Wagman, 1959) and at greater than zero, e.g. 50 msec (Boynton, Bush & Enoch, 1954; Bush, 1955; Boynton & Kandel, 1957). It is not entirely clear why these differences exist. However, both spectral characteristics of the flash and probe (Bush 1955) and pre-light adaptation condition (Boynton & Kandel, 1957; Bowen, Markell & Schoon, 1980) have been shown to influence the time of peak threshold elevation. The conditions closest to ours were probably those of Bush (1955) who found that peak threshold elevation occurred at 50 msec for a red probe on red flash.

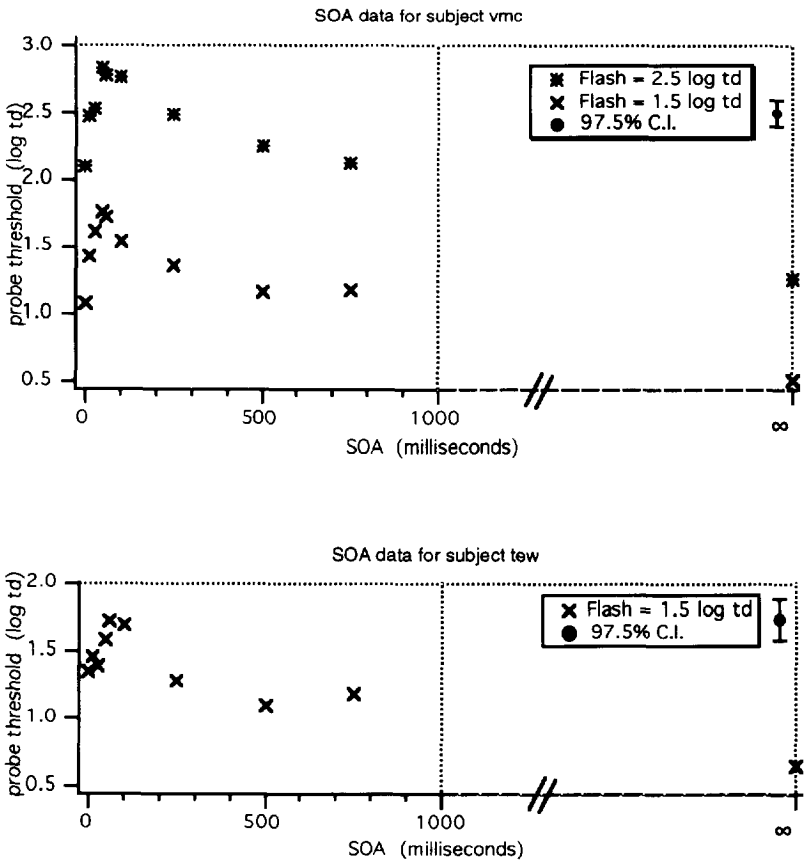

FIGURE 5. Experiment 3 results. Threshold vs SOA, parametric in illuminance. Each point is the average of five QUEST determinations of thresholds for observers VMC and three for observer TEW.

MODEL

The merged model proposed by Graham and Hood (1992b) consists of a frequency-dependent gain-controlling process, followed by a subtractive process, a static nonlinearity and some additional low-pass filtering. The model presented here (Fig. 6) follows this basic plan, differing most importantly in the initial component which determines the temporal frequency response. The first component [the parametrically controlled low-pass filter (pLPF) and control signal-generating LPF (cLPF)] is designed to simulate explicitly the data from the flicker experiment. We accomplished this using two second-order (quadratic) low-pass filters (described below) to model the pLPF. [Higher-order filters have been used by others to model psychophysical or physiological flicker data (e.g. Kelly, 1971; Tranchina & Peskin, 1988; Purpura, Tranchina, Kaplan & Shapley, 1990)]. The time constants of the filters and a scaling factor were derived from a control signal provided by a first-order low-pass filter fed by the input signal. We replaced the complete subtraction of the earlier merged model by a functionally equivalent high-pass filter. The compressive non-linear function (static non-linearity) was chosen to be linear near zero and odd-symmetric. The final stages of filtering present in Graham and Hood's model are not necessary in the current model (as discussed below).

The description of the model in Fig. 6 follows the periodic/aperiodic outline of Expts 1, 2, and 3. The parameters of the initial quadratic low-pass filters are first selected to match the flicker experiment data for each of the four backgrounds. A set of "parameter control" functions is then determined so that the model can tune the characteristics of the quadratic low-pass filters appropriately for arbitrary backgrounds. In this way the model is not limited to the four discrete background levels of the experimental data. The aperiodic data are then used to select an appropriate static non-linearity to match the observed response to shifts in the background away from the adapted level.

When completely developed, the model is embodied in a set of non-linear time-varying difference equations. We can compute predictions from this model to an arbitrary input by stepping through time in sufficiently small steps, calculating the difference equations at each step. We did compute predictions in this manner for Expts 1–3. Predictions were calculated for both "foreground signals" and "background signals". The foreground signal corresponds to the "target" field of the experiments [see Fig. 1(B)]. The background signal similarly corresponds to the "surround" field of the experiments. Each of these signals is passed through the same model. The decision process is based on a constant response criterion rule (constant ΔR rule) in which the response of the model to the background signal is subtracted from the response to the foreground. The stimulus is said to be detected when the peak of this difference (ΔR) is greater than or equal to a criterion value (δ).

Modeling the flicker data (Expt 1)

A prominent feature of the flicker data (Fig. 2) is the increase in corner frequency (sometimes referred to as the -3 dB frequency) as background level is increased. This feature, coupled with a tendency toward increased peakiness at higher background levels, led us to consider a multi-stage low-pass filter with staggered time constants to capture the shape of the response curves.

Beginning with Fuortes and Hodgkin (1964), a common approach has been to use a filter consisting of n identical stages each with the same time constant τ_c. The transfer function of such a filter is:

$$H(f) = \frac{\text{out}(f)}{\text{in}(f)} = \left(\frac{1}{\tau_c(j2\pi f) + 1}\right)^n, \quad (1)$$

$$\text{with } j = \sqrt{-1}.$$

With this approach, a corner frequency f_c and an attenuation rate (slope of the high-frequency fall-off) can be selected. (The attenuation rate is related to the number of stages n of the filter; the ultimate attenuation

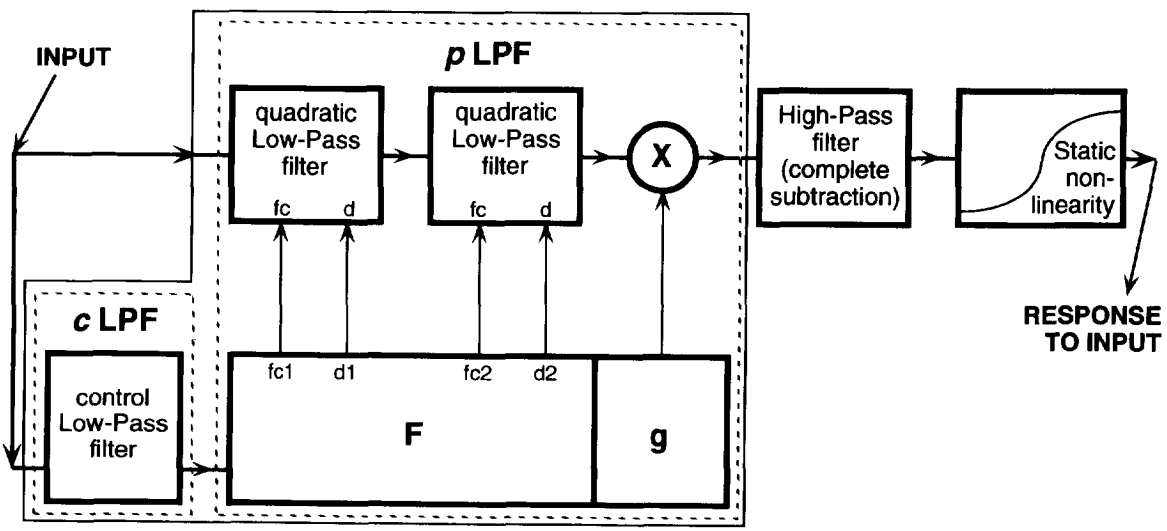

FIGURE 6. The merged model as developed in this paper. Two identical circuits are used in the simulations.

rate of a low-pass filter is n log units per decade when the slope of the transfer function is plotted on log–log axes.) However, with this approach the peakiness of the transfer function cannot be controlled. In fact, with such a filter there is no peak at all; one must introduce a high-pass filter into the circuit to create one. Another problem with using the equal τ_c filter [equation (1)] is that the slope to be fitted is rarely an exact integral number of log units per decade. Unfortunately, though specification of noninteger values of n may yield better fits, these "fractional order" systems are not achievable using physical components.

The general problem with the above filters is that by keeping all the time constants equal, one is pre-determining $n - 1$ of the controllable parameters. A better approach is to assign the individual time constants in a way that allows greater control over the shape of the frequency response. The special case of the second-order (quadratic) filter is especially appropriate because it can be described in terms of two parameters, the corner frequency f_c and the damping value d, which directly relate to our data. The transfer function for this filter is:

$$H(f) = \frac{(2\pi f_c)^2}{(j2\pi f)^2 + d2\pi f_c j2\pi f + (2\pi f_c)^2}. \quad (2)$$

[Note that a quadratic filter with $d = 2$ is equivalent to an equal-τ_c filter of equation (1) with $n = 2$.]

In the quadratic filter [equation (2)], f_c has its traditional meaning of "the frequency that separates the passband (less than f_c) from the attenuation band (greater than f_c)". The d value, when viewed in the frequency domain, determines the peakiness of the response near f_c. The d value also affects the initial attenuation rate upon entering the attenuation band. These two effects trade off: a steeper slope (steeper than the number of stages would imply) is obtained at the expense of a more peaky response. These tendencies are in concordance with the observed flicker data: the brightest background has a steeper slope and a peakier response.

Filter parameter fits. The number of low-pass stages needed to model our data will depend in part on the maximum slope observed in the flicker results of Fig. 2. In that data the steepest slope is about 5 log units per decade. At least five stages of equal-τ_c filtering would be required to attain this slope. By taking advantage of the trade-off between peakiness and attenuation rate, we can simplify the model by using two quadratic stages to create a fourth-order filter that closely matches the steepest slope in the data. Thus the transfer of the model includes two quadratic stages and a gain factor g and can now be expressed as

$$H(s) = g \cdot \left[\frac{\omega_{01}^2}{s^2 + d_1\omega_{01}s + \omega_{01}^2}\right] \cdot \left[\frac{\omega_{02}^2}{s^2 + d_2\omega_{02}s + \omega_{02}^2}\right] \quad (3)$$

with

$$s = j2\pi f;\ \omega_{0i} = 1/\tau_{0i} = 2\pi f_{ci}.$$

Figure 7 compares the fits of the transfer functions for the equal-τ_c filter of equation (1) [Fig. 7(A)] and the quadratic filter of equation (2) [Fig. 7(B)] to the data at four backgrounds. The parameters of each model were chosen for best fit to the four individual curves. It is apparent that the quadratic stages describe the data rather better than the equal-τ_c filter.

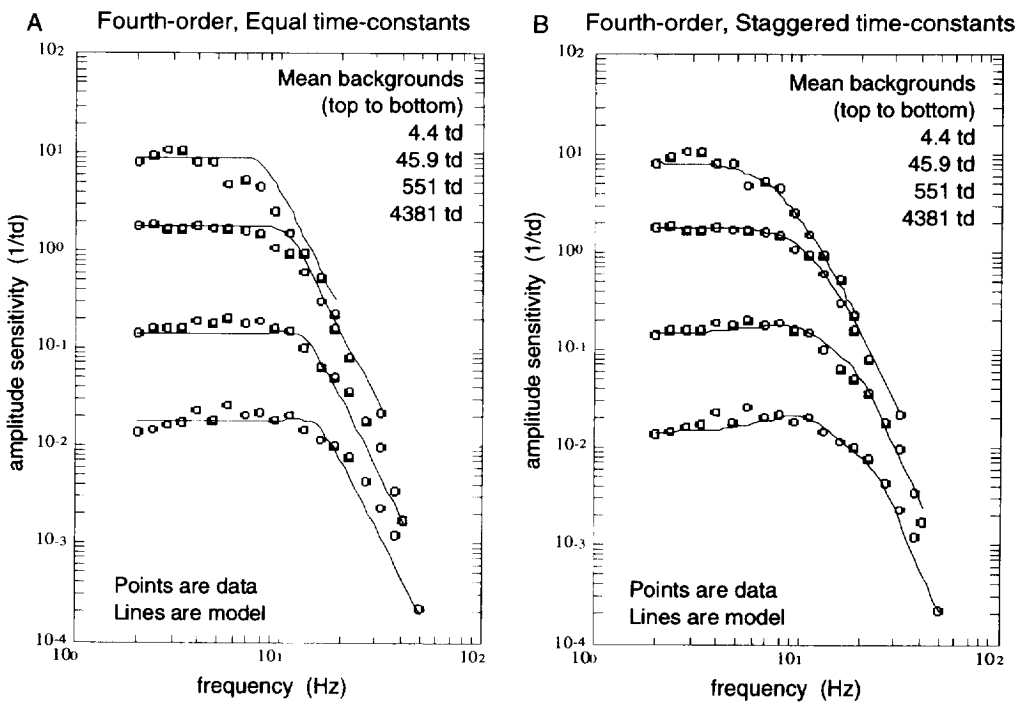

FIGURE 7. Filter fits to the periodic data for observer VMC. (A) Fit based on the equal-τ_c filter. (B) Fit based on the quadratic filters used in the present model.

Parameter control. The visual system must cope with a range of ambient light levels of which the four used in Expt 1 are merely a subset. Thus descriptive functions were chosen to allow interpolation for the five control parameters in equation (3) from the values we measured at four light levels to arbitrary levels.

The cLPF was a single-stage low-pass filter with a transfer function given by equation (1) with $n = 1$ and $\tau_c = 1.59$ sec yielding an f_c of 0.1 Hz. Letting $r_c(t)$ be its output, then the interpolated values for the five control parameters in equation (3) were computed as follows:

$$g = 2.2 \cdot [(45.899 + r_c(t))^{-0.641}] \cdot [(0.001 + r_c(t))^{-0.5114}] \quad (4)$$

$$z_c(r_c(t)) = 1/[1 + (r_c(t)/138.839)^{0.5}] \quad (5)$$

$$f_{c1}(t) = -4.299 \cdot z_c(t) + 11.65 \quad (6)$$

$$d_1(t) = -1.218 \cdot z_c(t) + 0.616 \quad (7)$$

$$f_{c2}(t) = -24.36 \cdot z_c(t) + 28.68 \quad (8)$$

$$d_2(t) = -1.003 \cdot z_c(t) + 0.448. \quad (9)$$

The high-pass filter and static nonlinearity. For the sake of completeness, the two remaining parts of the model are included though they do not materially affect the results of the simulation of the flicker experiment. The first of these elements is the complete subtraction, in the form of a first-order high-pass filter with a τ_c of 1.59 sec. This high-pass filter is equivalent to the more familiar low-pass filter and subtraction (Geisler, 1981, 1983; Adelson, 1982). The last element is the non-linear compressive function, which is essentially linear for near-threshold stimuli in the fully adapted state. With these elements in place, the model is complete as shown in Fig. 6.

Computational methods. In order to make the model computational, the output of the pLPF was expressed in terms of a set of differential equations using a state-space realization of the transfer-function description of the system in controller-canonical form (Kailath, 1980, especially Chaps 2 and 5; also see Wiegand, 1993 and MATLAB toolboxes). The outputs from the model were calculated numerically by changing all differential equations (for the cLPF, pLPF, and HPF) to difference equations and stepping through time in sufficiently small steps (programmed in MATLAB). In these simulations the time increment was set to 1/4096 sec based on preliminary calculations.

Computational results. To simulate a psychophysical threshold experiment we incorporated the constant ΔR rule into a binary search algorithm. Detection is assumed to have taken place when the difference between the foreground and background channels exceeds the threshold criterion value δ. The value of δ, which was set to 0.01 units in this experiment, determines the value of g that best fits the data. In simulating the flicker experiment, the model is considered to be "fully adapted" to a new background level after three τ_c (of the cLPF) have elapsed. At that time, the control filter output is only 0.022 log unit below its asymptotic value.

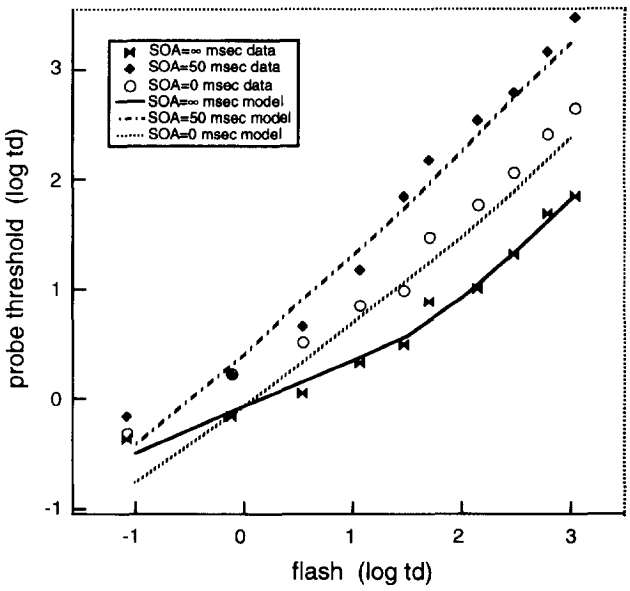

FIGURE 8. Fit of the model to the PF data at three SOAs for observer VMC. Included are the original data to be fitted (points) and the result of simulating the experiment on the model (lines).

In the flicker experiment simulation, the threshold was tested after 1 sec of a 2 sec presentation to account for the windowing effect as described earlier.

Modeling the probe-flash data in the fully adapted state (SOA = ∞)

Linear small-signal response. The comparison between flicker and probe-flash data for the fully adapted state (SOA = ∞) in Fig. 4 shows that the near-threshold response to either type of stimulus is the same to within a multiplicative constant. In the context of our model we can see that after the model adapts (i.e. after the background has been on for at least three τ_c of the cLPF), the filter parameters remain nearly constant. The 10 msec pulse has a frequency spectrum similar to that of an impulse: it is down less than 2 dB at 100 Hz and is very flat down to 0 Hz. When this impulse-like signal is passed through the peaky low-pass filter of the model the output is relatively richer in those frequency components that are accentuated by the resonant peak (about 7 Hz). This explanation of the comparison between results from the periodic and aperiodic experiments (Fig. 4) shows that many results from both traditions can be captured by a model that incorporates the correct temporal frequency characteristics.

Computational results. The solid line in Fig. 8 shows the results of the Expt 2 probe-flash simulation at SOA = ∞ [The data are repeated from Fig. 3(A)]. For this simulation $\delta = 0.02$. Recall that for the periodic predictions we used $\delta = 0.01$. This apparent difference is an artifact of our definition of threshold in the constant response criterion rule. The peak-to-peak signal present in the case of sinusoidal stimulation equals $2 \times \delta$. Consequently, we use $\delta = 0.01$ for periodic simulations (the flicker experiment) and $\delta = 0.02$ for aperiodic simulations (the probe-flash and SOA experiments).

Modeling the probe-flash data during and after flash onset

In the previous section the model performed in the "fully adapted" state. But, in the milliseconds after a large shift in the background level (SOA $\ll \infty$), all elements of the model play a part in determining the threshold. The remaining aperiodic simulations discussed below further test the model by calling into play the effects of the high-pass filter and the nonlinear compressive function.

The shape of the SOA curve depends on the pLPF, the cLPF and the signal's interaction with the static non-linearity (SNL). Two of these determinants, the cLPF and pLPF, have been fixed as described above. Only the choice of SNL remains for fitting the SOA data.

The choice of SNL is constrained by the necessity of achieving linearity for small signals. From this constraint it follows that the function should have odd symmetry (at least near zero) and be approximately linear near zero. In the present model we have chosen a logarithmic function as the basis of our SNL. Straightforwardly (as shown in Appendix A) we get the following SNL and parameters η and ω:

$$\mathrm{SNL} = \begin{cases} \omega \ln(1 + \eta x), & x \geq 0 \\ -\omega \ln(1 + \eta x), & x < 0 \end{cases} \tag{10}$$

with $\eta = 8.7334$ and $\omega = 0.1245$.

Threshold elevation at onset (SOA = 0). The non-linear compressive function, or SNL, is primarily responsible for the rise in threshold at the onset of the background flash. The early stages of the model respond to the onset of a flash (or other shift in background level) with a large extended pulse to the SNL. This extended pulse eventually settles down to zero due to the nulling action of the high-pass filter. However, any probe having an SOA under a few seconds will appear as a small perturbation riding on the much greater component which is due to the flash.

The effect of the SNL on the relatively small probe component of the signal can be thought of as a variable gain control in which the widely varying flash component acts as the control signal. The small probe signal is multiplied by the first derivative of the SNL, where this derivative is taken at a point along the curve specified by the flash signal:

$$r_p \cdot \left[\frac{\mathrm{dSNL}(r)}{dr}\right]_{r=r_f}. \tag{11}$$

Computational results. Figure 9 shows the fit of the model to the empirical SOA data points. The model describes the overall shape of the threshold vs SOA curves, including the peak at 50 msec. (See Appendix B for a further discussion of the 50 msec peak.)

Complete probe-flash results. With the determination of the SNL parameter, we are able to run a simulation of the complete set of probe-flash conditions. As shown above, the general shape of the TVI curve for the infinity condition was determined by the g function in the multiplicative stage of the model. The shape of the non-infinity curves is largely dependent on the rate of compression in the SNL [given by η in equation (10)].

Figure 8 shows the probe-flash simulation and the corresponding data. Note that the fit for the higher flash values is superior to that of the lower values. In the SOA = 0 msec case, the model seems to consistently predict thresholds about 0.15 log td below the empirical data. This is a result of fitting the parameter of the SNL at SOA = 50 msec and SOA = ∞. A better fit to the SOA = 0 msec data could be obtained with a compromise value for the SNL parameter. The low predictions for non-infinity thresholds for the -1 log td flash values are most likely due to the slow response of the pLPF when small flashes are presented on the fully-dark background. This can be remedied by either including a "dark noise" bias signal or by modifying the control function (F) to prevent the time constants of the pLPF from becoming too long in the fully dark state.

In a model which uses simple peak detection, such as ours, the detection of the probe component (of the signal from the model) can occur on the early part of the rising flash component. If the probe component is detected when it has not yet been driven out of the linear region of the SNL, the model will not produce a steeper slope

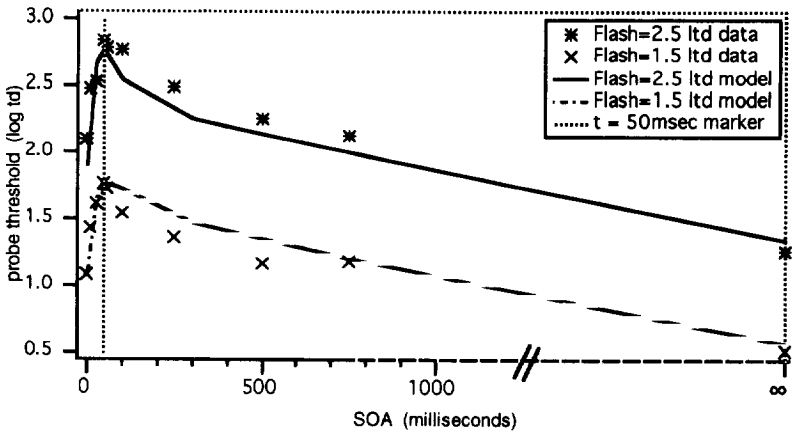

FIGURE 9. Fit of the model to the SOA data. Included are the original data to be fitted (points) and the result of simulating the experiment on the model (lines).

in the probe-flash SOA ≈ 0 condition. Because of this problem, Geisler (1979) proposed adding an extra LPF after the static non-linearity. In the earlier merged model (Graham & Hood, 1992b), it was necessary to use such a filter. In the present investigation we were able to sidestep this issue because, given the stimulus conditions we chose for the probe-flash experiment, our data simply did not exhibit a marked increase in slope for SOA ≈ 0.

DISCUSSION

Graham and Hood (1992b) showed that a merged model of light adaptation could be made to qualitatively fit data collected in the periodic and aperiodic traditions. Here we have shown that it is possible to make a merged model quantitatively fit experimental data from both traditions if the data is collected from the same observer in the same experimental situation. This model has passed the test of exhibiting the background-onset effect and high-frequency linearity.

Our model bears certain similarities to the models from the periodic tradition, especially those which contain linear, time-varying filters (e.g. Sperling & Sondhi, 1968). Although these models can predict a range of phenomena, they cannot be made to exhibit the proper background-onset effect (Graham & Hood, 1992b). Many of these models achieve their parameter control with feedback and feedforward signals within the model. In our present model we took a different approach.

In our model most of the functionality is based on the action of the pLPF. Periodic characteristics of the model such as the peakiness, change in attenuation rate, and high-frequency linearity, are accommodated primarily by allowing unequal time constants in the pLPF. Moreover, using this method, we did not have to resort to introducing a high-pass element to produce the observed peakiness, thus simplifying the model. With its control signal fixed, the pLPF can begin to account for small-signal thresholds from both types of experiments. The dynamic changes of the thresholds in response to shifts in the background are accommodated by allowing the control signal (from the cLPF) to vary the parameters of the pLPF. Thus the response in the fully adapted aperiodic condition (SOA $= \infty$) follows naturally from the filter parameters fitted in the steady state and the response for the SOA $< \infty$ conditions fall in line with proper selection of the SNL.

Peak at 50 msec

The maximum threshold elevation in our aperiodic experiments occurred at SOA = 50 msec for both backgrounds (see discussion after Expt 3). Earlier attempts to model aperiodic data had also shown a maximum threshold elevation at $0 <$ SOA $< \infty$ msec (Graham & Hood, 1992b). The stable position of the 50 msec peak threshold elevation was subsequently captured in the current model by the dynamically varying filter (pLPF) and nonlinear compressive function (SNL).

Impulse responses

The model here has implications for attempts to determine the impulse response of the visual system. Many previous attempts to determine an impulse–response function are based on the assumption that the eye is a linear time-invariant system as long as the background level is held constant (e.g. Ikeda, 1965; Swanson *et al.*, 1987; Dagnelie, 1992; Tyler, 1992). In this study, we successfully used a time-varying filter to predict a range of phenomena, raising questions about the utility of describing the system in terms of its impulse response: if the eye is not a linear time-invariant system, the impulse response is necessarily a complicated and changing entity.

Limitations and extensions

Our model was able to predict the data of our experiments using similar time constants (of just under 2 sec) for both the subtractive (HPF) and the multiplicative gain (cLPF) processes. In general, other researchers have found longer time-constants for their subtractive processes than for their multiplicative processes (Shevell, 1977; Hayhoe *et al.*, 1987; Walraven & Valeton, 1984; Hayhoe, Levin & Koshel, 1992; Olson, Tulunay-Keesey & Saleh, 1993). The estimates of the time-course of the subtractive process have ranged from approx. 2 to 10 sec or more. Our subtractive process is roughly consistent with this finding. The time-constant of their multiplicative process has generally been found (e.g. Hayhoe *et al.*, 1987; Hayhoe, 1992) to be much faster than the time constant of our cLPF. Our model might need a faster cLPF time constant to predict data from these studies. Because the performance of our model does not appear to be especially sensitive to manipulation of these time constants, such changes are unlikely to significantly degrade the performance of our model under the conditions addressed in this study.

Other psychophysical paradigms. To account for differences between time–courses of light and dark adaptation, the model would have to be extended, perhaps by incorporating some form of rectification and storage of the control signal from the cLPF. This modification would be easy to implement based on data from an appropriate experiment. Boynton, Sturr and Ikeda (1961), using a flickering background field, showed that the increment threshold followed a 30 Hz background even when the 30 Hz modulation was not perceptible. Using some variant on this technique, the mean threshold elevations produced by a periodically-varying background could be explored and the data used to inform the design of the control signal rectification and storage stage. More recently, Robson and Powers (1989) and Chase, Wiegand, Hood and Graham (1993) have explored the same paradigm.

There are a variety of other paradigms that could be explored (in the context of our consistent stimulus conditions) as challenges for our model. Threshold elevations at background offset, as described by Crawford (1947), can be accommodated by our model

with minor modification of the cLPF output signal as described in the previous paragraph, or by introducing an asymmetrical SNL. More recent work (e.g. Bowen, Pokorny & Smith, 1989; Kremers, Lee, Pokorny & Smith, 1991a, b, 1993; Bowen, Pokorny, Smith & Fowler, 1992), using sawtooth and other compound periodic waveforms has more generally shown that thresholds for rapid-off stimuli tend to be lower than for rapid-on. This asymmetry has been used as evidence of sensitivity to the phase information present in the stimuli. Further development of our model based on these results may warrant the inclusion of multiple channels with different temporal-phase characteristics.

Noise. Our model is totally deterministic in that it exhibits no noise in its responses. The effects of noise or other probabilistic processes could be added. These considerations are usually linked to the type of decision rule chosen (Graham & Hood, 1992a), but can also help the current model to achieve a limiting sensitivity level in the mesopic range by simulating dark noise (Barlow & Sparrock, 1964). This is a way of halting the downward trend in the thresholds exhibited by our model as it leaves the photopic range it was designed to cover.

Single-channel assumption. One further limitation of our model is that we assume a single spatial, chromatic and temporal channel (photopic range, long wavelength, foveal stimulation). To predict a wider range of results, one would obviously have to incorporate additional channels.

Conclusion

A merged model that includes a time-varying, staggered time-constant low-pass filter can account for many of the characteristics observed in data from experiments in both the periodic and aperiodic traditions.

REFERENCES

Adelson, E. H. (1982). Saturation and adaptation in the rod system. *Vision Research, 22*, 1299–1312.

Barlow, B. H. & Sparrock, J. M. B. (1964). The role of afterimages in dark adaptation. *Science, 144*, 1309–1314.

Battersby, W. S. & Wagman, I. H. (1959). Neural limitations of visual excitability. I. The time course of monocular light adaptation. *Journal of the Optical Society of America, 49*, 752–759.

Bowen, R. W., Markell, K. A. & Schoon, C. M. (1980). Two-pulse discrimination and rapid light adaptation: Complex effects on temporal resolution and a new visual temporal illusion. *Journal of the Optical Society of America, 70*, 1453–1458.

Bowen, R. W., Pokorny, J. & Smith, V. C. (1989). Sawtooth contrast sensitivity: Decrements have the edge. *Vision Research, 29*, 1501–1509.

Bowen, R. W., Pokorny, J., Smith, V. C. & Fowler, M. A. (1992). Sawtooth contrast sensitivity: Effects of mean illuminance and low temporal frequencies. *Vision Research, 32*, 1239–1248.

Boynton, R. M. & Kandel, G. (1957). On responses in the human visual system as a function of adaptation level. *Journal of the Optical Society of America, 47*, 275–286.

Boynton, R. M., Bush, W. R. & Enoch, J. M. (1954). Rapid changes in foveal sensitivity resulting from direct and indirect adapting stimuli. *Journal of the Optical Society of America, 44*, 56–60.

Boynton, R. M., Sturr, J. F. & Ikeda, M. (1961). Study of flicker by increment threshold technique. *Journal of the Optical Society of America, 51*, 196–201.

Bush, W. R. (1955). Foveal light adaptation as affected by the spectral composition of the test and adapting stimuli. *Journal of the Optical Society of America, 45*, 1047–1057.

Chase, V. M., Wiegand, T. E., Hood, D. C. & Graham, N. (1993). Exploring the dynamics of light adaptation using a sinusoidally modulated background and a probe. *Investigative Ophthalmology and Visual Science, 34*, 1036.

Craik, K. J. (1938). The effect of adaptation on differential brightness discrimination. *Journal of Physiology, 92*, 406–421.

Crawford, B. H. (1947). Visual adaptation in relation to brief conditioning stimuli. *Proceedings of the Royal Society of London, B, 134*, 283–302.

Dagnelie, G. (1992). Temporal impulse responses from flicker sensitivities: Practical considerations. *Journal of the Optical Society of America, 9*, 659–672.

Finkelstein, M. A. & Hood, D. C. (1981). Cone system saturation: More than one stage of sensitivity loss. *Vision Research, 21*, 319–328.

Finkelstein, M. A., Harrison, M. & Hood, D. C. (1990). Sites of sensitivity control within a long-wavelength cone pathway. *Vision Research, 30*, 1145–1158.

Fuortes, M. G. F. & Hodgkin, A. L. (1964). Changes in time scale sensitivity in the ommatidia of Limulus. *Journal of Physiology, 172*, 239–263.

Geisler, W. S. (1978). Adaptation, afterimage and cone saturation. *Vision Research, 18*, 279–289.

Geisler, W. S. (1979). Initial image and afterimage discrimination in the human rod and cone systems. *Journal of Physiology, 294*, 165–179.

Geisler, W. S. (1981). Effects of bleaching and backgrounds in the flash response of the cone system. *Journal of Physiology, 312*, 413–434.

Geisler, W. S. (1983). Mechanisms of visual sensitivity: Backgrounds and early dark adaptation. *Vision Research, 23*, 1423–1432.

Graham, N. (1989). *Visual pattern analyzers*. New York: Oxford University Press.

Graham, N. & Hood, D. C. (1992a). Modeling the dynamics of light adaptation: The merging of two traditions. *Vision Research, 23*, 1373–1393.

Graham, N. & Hood, D. C. (1992b). Quantal noise and decision rules in dynamic models of light adaptation. *Vision Research, 32*, 779–787.

Hayhoe, M. M. (1990). Spatial interactions and models of adaptation. *Vision Research, 30*, 957–965.

Hayhoe, M., Benimoff, N. I. & Hood, D. C. (1987). The time-course of multiplicative and subtractive adaptation processes. *Vision Research, 27*, 1981–1996.

Hayhoe, M. M., Levin, M. E. & Koshel, R. J. (1992). Subtractive processes in light adaptation. *Vision Research, 32*, 323–333.

Hood, D. C. (1978). Psychophysical and electrophysiological tests of physiological proposals of light adaptation. In Armington, J., Krauskopf, J. & Wooten, B. (Eds), *Visual psychophysics: Its physiological basis* (pp. 141–155). New York: Academic Press.

Hood, D. C. & Finkelstein, M. A. (1986). Sensitivity to light. In Boff, K. R., Kaufman, L. & Thomas, J. P. (Eds), *Handbook of perception and human performance, Vol. I: Sensory processes and perception* (pp. 5-1–5-66). New York: Wiley.

Hood, D. C., Finkelstein, M. A. & Buckingham, E. (1979). Psychophysical tests of models of the response function. *Vision Research, 19*, 401–406.

Hood, D. C., Ilves, T., Wandell, B. & Buckingham, E. (1978). Human cone saturation as a function of ambient intensity: A test of models of shifts in the dynamic range. *Vision Research, 18*, 983–993.

Ikeda, M. (1965). Temporal summation of positive and negative flashes in the visual system. *Journal of the Optical Society of America, 55*, 1527–1534.

Ives, H. E. (1992). A theory of intermittent vision. *Journal of the Optical Society of America, 6*, 343–361.

Kailath, T. (1980). *Linear systems*. New Jersey: Prentice-Hall.

Kelly, D. H. (1959). Effects of sharp edges in a flickering field. *Journal of the Optical Society of America, 49*, 730–732.

Kelly, D. H. (1969). Diffusion model of linear flicker responses. *Journal of the Optical Society of America, 59*, 1665–1670.

Kelly, D. H. (1971). Theory of flicker and transient responses, I: Uniform flicker. *Journal of the Optical Society of America, 61*, 537–546.

Kelly, D. H. (1972). Adaptation effects on spatio-temporal sine-wave thresholds. *Vision Research, 12*, 89–101.

Kremers, J., Lee, B. B., Pokorny, J. & Smith, V. C. (1991a). Linear analysis of macaque ganglion cell responses to complex temporal waveforms. *Investigative Ophthalmology and Visual Science (Suppl.), 32*, 1090.

Kremers, J., Lee, B. B., Pokorny, J. & Smith, V. C. (1991b). The responses of macaque retinal ganglion cells to complex temporal waveforms. In Valberg, A. & Lee, B. B. (Eds), *From pigments to perception; advances in understanding the visual process* (pp. 173–177). London: Plenum Press.

Kremers, J., Lee, B. B., Pokorny, J. & Smith, V. C. (1993). Responses of macaque ganglion cells and human observers to compound periodic waveforms. *Vision Research, 33*, 1997–2011.

Lamb, T. D. & Pugh, E. N. (1992). A quantitative account of the activation steps involved in phototransduction in amphibian photoreceptors. *Journal of Physiology, 449*, 719–758.

Landis, C. (1953). An annotated bibliography of flicker fusion phenomena. In *Ann Arbor: Armed Forces National Research Council Vision Committee Secretariat.*

de Lang, H. (1952). Experiments on flicker and some calculations on an electrical analogue of the foveal systems. *Physica, 18*, 935–950.

de Lange, H. (1958). Research into the dynamic nature of the human fovea–cortex systems with intermittent and modulated light. *Journal of the Optical Society of America, 48*, 779–789.

Olson, J. D., Tulunay-Keesey, Ü. & Saleh, B. E. A. (1993). Fading time of retinally-stabilized images as a function of background luminance and target width. *Vision Research, 33*, 2127–2138.

Purpura, K., Tranchina, D., Kaplan, E. & Shapley, R. M. (1990). Light adaptation in the primate retina: Analysis of changes in gain and dynamics of monkey retinal ganglion cells. *Vision Neuroscience, 4*, 75–93.

Robson, J. G. (1966). Spatial and temporal contrast sensitivity functions of the visual system. *Journal of the Optical Society of America, 56*, 1141–1142.

Robson, J. G. & Powers, M. K. (1989). Sensitivity changes induced by temporal modulation of a background. Talk at Optical Society of America and personal communication.

Roufs, J. A. J. (1972a). Dynamic properties of vision—I. Experimental relationship between flicker and flash thresholds. *Vision Research, 12*, 261–278.

Roufs, J. A. J. (1972b). Dynamic properties of vision—II. Theoretical relationship between flicker and flash thresholds. *Vision Research, 12*, 279–292.

Shapley, R. M. & Enoch-Cugell, C. (1984). Visual adaptation and retinal gain controls. *Progress in Retinal Research, 3*, 263–343.

Shevell, S. K. (1977). Saturation in human cones. *Vision Research, 17*, 427–434.

Sperling, G. & Sondhi, M. M. (1968). Model for visual luminance discrimination and flicker detection. *Journal of the Optical Society of America, 58*, 1133–1145.

Swanson, W. H., Ueno, T., Smith, V. C. & Pokorny, J. (1987). Temporal modulation sensitivity and pulse detection thresholds for chromatic and luminance perturbations. *Journal of the Optical Society of America, 4*, 1992–2005.

Tranchina, D. & Peskin, C. S. (1988). Light adaptation in the turtle retina: embedding a parametric family of linear models in a single nonlinear model. *Visual Neuroscience, 1*, 339–348.

Tranchina, D., Sneyd, J. & Cadenas, I. D. (1991). Light adaptation in turtle cones: Testing and analysis of a model for phototransduction. *Biophysical Journal, 60*, 217–237.

Tyler, C. W. (1992). Psychological derivation of the impulse response through generation of ultrabrief responses: Complex inverse estimation without minimum-phase assumptions. *Journal of the Optical Society of America, 9*, 1025–1041.

Van Nes, F. L., Koenderink, J. J., Nas, H. & Bouman, M. A. (1967). Spatio-temporal modulation transfer function in the human eye. *Journal of the Optical Society of America, 57*, 1082–1088.

Walraven, J. & Valeton, J. M. (1984). Visual adaptation and response saturation. In Van Doorn, A. J., Van de Grind, W. A. & Koenderink, J. J. (Eds), *Limits in perception* (pp. 401–429). Utrecht: VNU Science Press.

Watanabe, T., Mori, N. & Nakamura, F. (1992). A new superbright LED stimulator: Photodiode-feedback design for linearizing and stabilizing emitted light. *Vision Research, 32*, 953–961.

Watson, A. B. (1986). Temporal sensitivity. In Boff, K. R., Kaufman, L. & Thomas, J. P. (Eds), *Handbook of perception and human performance, Vol. I: Sensory processes and perception.* New York: Wiley.

Watson, A. B. & Pelli, D. G. (1983). QUEST: A Beysian adaptive psychometric method. *Perception and Psychophysics, 33*, 113–120.

Westheimer, G. (1966). The Maxwellian view. *Vision Research, 6*, 669–682.

Wiegand, T. E. (1993). A psychophysically based computational model of the dynamics of light adaptation. Doctoral dissertation, Columbia University. Ann Arbor: University Microfilms International.

Acknowledgements—This research was supported by National Eye Institute grants EY-08459 and EY-02115 to N. Graham and D. Hood respectively. We thank Joel Pokorny and Bill Swanson for their assistance in constructing the PDM stimulator. We also thank Ben Sachtler for assisting in the proofreading process.

APPENDIX A

Derivation of the SNL

In the present model we have chosen a logarithmic function as the basis of our SNL

$$\omega \ln(1+\eta x). \tag{A1}$$

The series expansion of this function,

$$\omega\eta x + \sum_{k=2}^{\infty} \frac{\omega}{k} (\eta x)^k (-1)^{k+1} \tag{A2}$$

shows that it is strongly linear near zero. Taking the derivative of the proposed function with respect to x we see that it has the required "compressive" property

$$\frac{\omega\eta}{(1+\eta x)}. \tag{A3}$$

The value of this derivative (interpreted as the slope or gain of the SNL at a particular x value) decreases for increasing x values. The rate at which the gain decreases is controlled by the value of η. Also, it is a simple matter to solve for a value of ω that gives any desired gain near zero. Because ω is expressed in terms of η, the resulting SNL has only one free parameter

$$\text{gain}_0 = \frac{\omega\eta}{(1+\eta x)}; \quad \omega = \frac{\text{gain}_0}{\eta} + \text{gain}_0 x. \tag{A4}$$

Fitting this free parameter is fairly straightforward. The earlier stages of the model produce a signal that has a probe component and a flash (background) component as described previously. The general shape component follows the desired shape of the response of the model to the SOA experiment. The only "shaping" of the response remaining to be performed by the SNL is to scale the magnitude of the effect of SOA on the threshold.

This threshold elevation is at its peak at 50 msec and is non-existent at infinity. We begin fitting by noting that at infinity the flash component of the input to the SNL is zero, that is, the total response to an at-threshold input to the model is equal to δ. (This follows from the earlier fit of the gain function to the periodic data.) Since this response already yields the proper behavior at SOA $= \infty$, the SNL should apply a gain of 1 to these small signals. Thus we have determined

$$\omega = \frac{1}{\eta} + x \tag{A5}$$

as the coefficient of the SNL. As long as the coefficient ω follows the above relation (with $0 < x < \delta$ here we choose $x = 0.01$) the value of η can be varied independently of the small-signal characteristic.

The value of η can be determined by solving for it in the system

$$\begin{cases} \omega \ln(1 + \eta a) - \omega \ln(1 + \eta b) = \delta \\ \omega \ln(1 + \eta c) - \omega \ln(1 + \eta d) = \delta \end{cases} \quad \text{(A6)}$$

where a and c are the peak pre-SNL responses of the model to an SOA = 50 msec probe at threshold for the two flash levels we are trying to fit and where b and d are the corresponding responses to the flash only (i.e. the background channel responses). This system is difficult to solve analytically because it involves transcendental functions of η in an essentially non-algebraic way. However, it is a simple matter to find a numerical solution using a computer, and thus we have determined the value of η to be 8.7334, from which it follows that $\omega = 0.1245$ using the following values for the constants in the system of equations: $a = 19.008$, $b = 16.1739$, $c = 5.4669$, $d = 4.6381$, $\delta = 0.02$.

Our function for the SNL in equation (A1) can be made to be odd-symmetric by defining our SNL as

$$\text{SNL}(x) = \begin{cases} \omega \ln(1 + \eta x), & x \geq 0 \\ -\omega \ln(1 - \eta x), & x < 0 \end{cases} \quad \text{(A7)}$$

The fact that the basic function $f(x)$ and the $-f(-x)$ extension both have the same first derivative at zero assures that both the resulting function and its derivative are piecewise continuous through the region of the splice. Thus, the model will not exhibit pathological behavior due to this method of producing an odd function.

The static nonlinearity of equation (A7) does not saturate but rather produces log probe threshold vs log flash intensity curves of constant asymptotic slope. To handle the saturation observed by some at high flash intensities, one would need to modify this static non-linearity to asymptotically saturate as opposed to being only compressive.

APPENDIX B

Understanding the 50 msec peak

At abrupt transitions in background level, the probe signal is modified by the time-varying nature of the pLPF (as well as by the gain-controlling aspect of the SNL). The effect of this modification is hard to study analytically because this filter is not a "linear time-invariant system" and is not subject to the simplifying theorems that apply to such filters. In order to examine the origin of the stable 50 msec elevation it is productive to perform a short experiment on the model.

If we fix the control signal $r_c(t)$ at the fully adapted value and do not allow it to vary, the peak threshold elevation changes its temporal position with changes in flash intensity. This is consistent with the filter tuning for each adapted value but is not what we observed in the SOA experiment. If we allow the parameters of the pLPF to vary dynamically according to the control signal (as in our model), the peak threshold remains close to 50 msec as observed experimentally. This result demonstrates that the stable peak at 50 msec is related to the effects of the non-time-invariance of the pLPF.